UDK 620.1:621.791:669.715:67.017
Original scientific article/Izvirni znanstveni članek

ISSN 1580-2949
MTAEC9, 55(5)693(2021)

EFFECT OF TOOL-PIN PROFILES OVER SQUARE-WAVE TOOL-PATH PATTERN ON THE FRICTION-STIR WELDING OF AA6061-CU DISSIMILAR ALLOYS

VPLIV PROFILA TRNA ORODJA NA MEDSEBOJNO VARJENJE PLOŠČ Z GNETENJEM IZ Al ZLITINE AA6061 IN BAKRA PRI POTOVANJU ORODJA V OBLIKI KVADRATNIH VALOV

Loganathan Prabhu[1*], Satish Shanmugam[2], Thiagarajan Chandrasekaran[3]

[1]Department of Mechanical Engineering, SatyabamaInstitute of Science and Technology
[2]Department of Mechanical Engineering, Velammal Engineering College
[3]Department of Mechanical Engineering, AarupadaiVeeduInstitute of Technology

Prejem rokopisa – received: 2021-06-23; sprejem za objavo – accepted for publication: 2021-07-19

doi:10.17222/mit.2021.202

In the present work, the friction-stir welding of Al6061-annealed pure copper dissimilar metals with square-wave tool-pin movement pattern was investigated. The aim of this experiment was to identify the significant effect of square-wave tool movement, along with three different tool-pin profiles, on friction stir welding. Different tool-pin profiles of square, round and hexa-spiral shapes were selected and their significant outcomes were revealed. Friction-stir-welding parameters including tool rotations of 1500 min^{-1} and 2000 min^{-1}, tool-pin-movement step sizes of 1.0 mm and 2.0 mm and weaving rates of 100 mm/min and 150 mm/min were selected. The advantages of the tool-movement pattern and tool-pin profile shape were examined with mechanical testing and a microstructure analysis. The mechanical results showed that the tool rotation of 1500 min^{-1}, step size of 1.0 mm, welding rate of 150 mm/min and the square-tool pin-profile give better mechanical properties. Microstructural results revealed a better grain refinement and a uniform dispersion of microconstituents resulting from the implementation of the square-wave tool-pin movement pattern along with the square-tool pin profile. The EDAX report confirmed that the weld nugget contained both aluminum and copper in equal percentages, indicating fine mixing of the two parent metals.

Keywords: friction-stir welding, square-wave pattern, pin profile, X-ray, microstructure

V članku je opisan proces medsebojnega varjenja plošč iz Al zlitine Al6061 in čistega žarjenega bakra, s postopkom varjenja z gnetenjem. Pri tem je, vrteči se trn oziroma čep naprave za varjenje, potoval po ploščah v obliki vzorca kvadratnih valov. Cilj te eksperimentalne raziskave je bil, da se ob uporabi treh različnih profilov trnov orodja, ugotovi pomen te vrste gibanja trna in kakšen je vpliv na sam proces varjenja. Izbrane oblike profilov trnov orodja za varjenje so bile: kvadratna, okrogla in petkraka. Izbrani parametri postopka varjenja z gnetenjem so bili: hitrost vrtenja trna (1500 min^{-1} in 2000 min^{-1}), korak gibanja (1,0 mm in 2,0 mm), hitrost varjenja (100 mm/min. in 150 mm/min.). Prednosti izbrane oblike in načina gibanja trna orodja so analizirali s pomočjo izvedenih mehanskih preizkusov in mikrostrukturne analize. Rezultati mehanskih preizkusov so pokazali, da je, kombinacija procesnih parametrov 1500 min^{-1}, korak 1,0 mm in hitrost varjenja 150 mm/min. s kvadratnim profilom trna, dala najboljše mehanske lastnosti zvarov. Rezultati mikrostrukturnih preiskav so pokazali najboljše udrobljenje mikrokristalnih zrn in enakomerno porazdelitev mikrostrukturnih sestavin pri uporabi kvadratnega profila trna in njegovem potovanju po poti kvadratnih valov. Analize z rentgensko energijsko disperzijsko spektroskopijo (EDAX) so potrdile, da nastali zvarni spoj vsebuje v enaki količini oba kemijska elementa; to je aluminij in baker, kar potrjuje dobro medsebojno mešanje dveh dokaj težko združljivih materialov.

Ključne besede: varjenje z gnetenjem, vzorec kvadratnih valov, profil trna orodja, rentgenski žarki, mikrostruktura

1 INTRODUCTION

Friction-stir welding is a pollution-free, solid-state welding technique where metals are joined with frictional heat and pressure.[1,2] A rotating tool rotates over a specimen at desired revolutions and as a result, frictional heat develops and the metal gets plasticized. Plasticized metals are joined with the help of pressure. The need for lightweight aluminum products in the aircraft, automobile and construction industries is increasing day by day. The automobile sector is making attempts to replace iron products with lightweight aluminum ones to improve their product efficiency. Joining non-ferrous metals using friction-stir welding is the foremost method, during which similar and dissimilar metals are joined and energy-saving parameters are observed, which is very important nowadays.

The weld quality in an FSW process depends greatly on the workpiece metal, weaving speed, tool rotation and degree of intermixing of parent metals.[3,4] The tool-pin movement can also play a vital role in the intermixing of parent metals, which is directly proportional to the strength of weldments. Welding of similar alloys has a low degree of complexity, whereas welding of dissimilar alloys is more complicated due to the mismatch of the cooling rates.[5] At a high melting temperature, metal cools down more rapidly than at a low melting temperature, thus requiring special parameters. High frictional

*Corresponding author's e-mail:
prabhu.phd2012@gmail.com (L. Prabhu)

heat at a low speed provides for good quality weldments with a low energy consumption. Generally, in FSW, the tool rotates and moves in a straight line, whereas with the square wave pattern method, the tool moves in both x and y directions, thus making the intermixing of parent metals possible. With complete intermixing of parent metals, the microconstituents are dispersed throughout the matrix. This allows the improvement of mechanical properties through precipitated strengthening.[6,7] A fine intermixing of parent metals can also be achieved with an appropriate tool-face profile. Hence, round, square and spiral tool pin profiles can be used as stir tools. Zhang et al.[8] confirmed that dissimilar metals formed with friction-stir welding exhibit better tensile strength than that of the Al base metal. They also indicated the formation of micro-elements like Al_4Cu_9 and Al_2Cu on the nugget as a result of short-circuit cooling. Bisadi et al.[9] reported on dissimilar parameters for friction-stir welding of Al and Cu. They found that weldments were in good condition at low tool-rotational speeds, whereas defects developed when the tool speed increased. The latter was due to improper fusion and cooling.

An important factor to be addressed in achieving robust welding joints is the influence of the tool movement. The flowability of the material during the stirring action of forward and retracting movements of the instrument influences the improved mechanical and microstructural properties. Several studies on the impact of tool-path management on the nugget zone with regard to improved welding qualities were carried out.

D. Jayabalakrishnan et al.[10] explored the novel tool-path pattern for combining dissimilar aluminium and copper alloys, using the eccentric weave motion in the nugget zone. Their studies showed that, with an increase in the weaving time, dynamic recrystallization of grain limits is created to achieve IMC, which strengthens different joints.

M. Balasubramanian et al.[11] further developed the study about the effects of welding on the fabric path through the effect of the pin offset on increasing the fabric radius. They concluded that sound welding is achieved with the optimum 1-mm pin offset in weave welding. However, because of the increased weaving radius due to the pin offset, the formation of tunnel defects increased.

A research on the FSW joining of AA5754 alloys with an orbital motion was conducted by Cabibo et al.[12] Their findings showed that by increasing the weave radius along the way, grain borders are efficiently stirred to reduce the coarse oxide formation. This may cause the welding surface to peel off and lose its cohesion.

In order to avoid such defects, the weaving radius must be reduced by designing a new geometry with a small step for weaving. This work is therefore a new study of the geometric tool-path pattern with a quadratic weave of different step sizes. The formation of equiaxed grains can result in effective dynamic recrystallization.

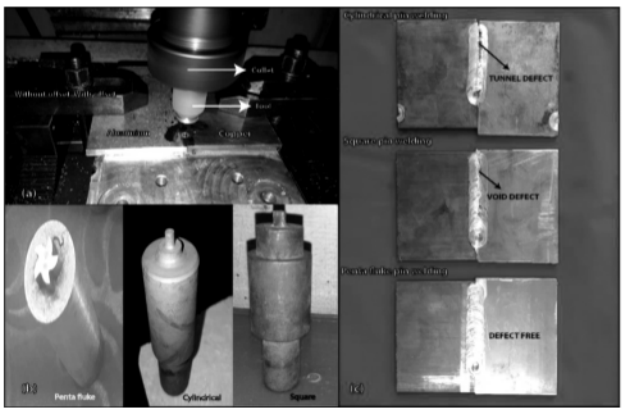

Figure 1: a) FSW set-up on VMC, b) FSW tool dimensions, c) mechanical clamping of Al-Cu plates on VMC

2 EXPERIMENTAL PART

2.1 Materials

The aluminum used for this study was AA6061 (150 mm × 150 mm), containing in *w*/% (0.9 Mg, 0.62 Si, 0.28 Cu, 0.17 Cr, 0.33 Fe, 0.02 Zn, 0.06 Mn, 0.02 Ti) and the rest was Al. The copper used for this study was annealed pure copper. **Table 1** shows the mechanical properties of the parent metals. The tool material used for this study was HSS.

Table 1: Mechanical properties of the workpiece materials

S. No.	Material	Tensile strength (MPa)	Elongation (%)	Izod impact (J)	Microhardness (HV)
1	AA6061	280	15	105	18
2	Copper	206	25	73	26

2.2 Procedure

Square-shaped 6-mm sheets of AA6061 and copper were placed on the workbed as a butt-joint configuration in a vertical milling center (VMC) with the help of mechanical clamps. **Figure 1c** shows the mechanical clamping of the Al-Cu dissimilar metal plates. Machining was started at one end, based on the process parameters. **Figure 1a** shows the experimental set-up with tools. **Figure 1b** shows the FSW tool-pin profile with its dimensions. It was noted that the difference between the pin diameter and shoulder diameter was 4 mm, reducing the width of the weld bead. **Figure 2a** shows different step sizes of the tool movement pattern. A constant axial load of 6 kN was applied throughout the process. Welding was performed with three different tool-pin profiles. The welded samples were visually inspected for defects after the completion of the post-cleaning process.

2.3 Preparation of specimens

For various tests, cleaned welding components were cut in accordance with the ASTM standards. Samples

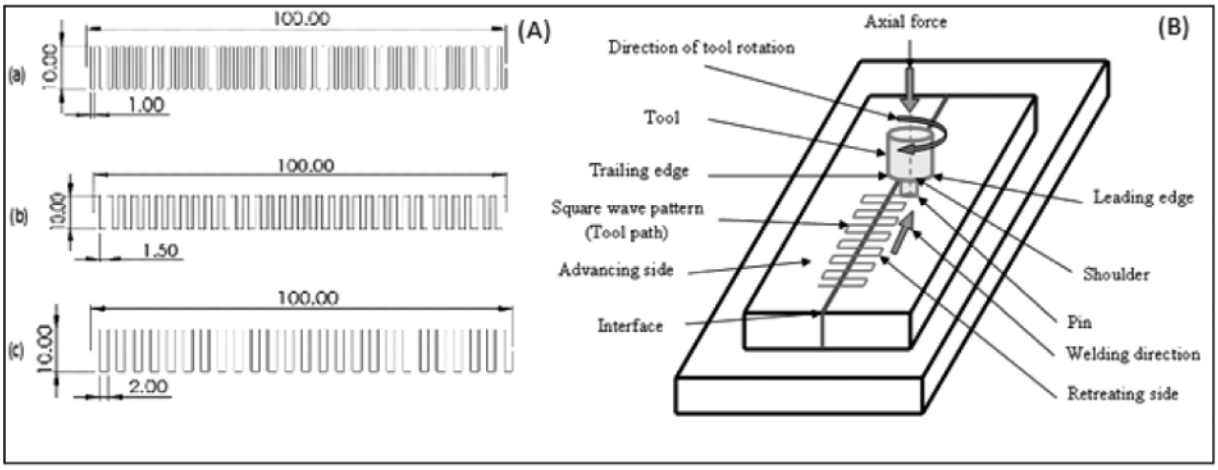

Figure 2: a) step sizes of tool-pin movement patterns, b) schematic diagram of square-wave tool-pin movement pattern

were cut to the required dimensions, with an abrasive 1-mm-diameter water jet, 80 mesh garnet; the flow rate was 0.35 kg/min and the maximum pressure was 510 MPa. Pre-testing dimensional precision was checked for the sectioned specimens.

2.4 Mechanical characterization

ASTM E8M-04 was used for tensile-strength tests of the welded components. For the estimation of the tensile properties of the welded samples, we used a universal testing machine (MTS C44, India) with a 40-T capacity and a cross-head speed of 1.5 mm/min. Samples with a 50-mm length and 12.5-mm width were used. A tensile test on the basis of ASTM E23 was carried out. Five identical samples were tested and average values were calculated for each property. ASTM 256 and an Izod-impact tester (Kristal, India) with a capacity of 30 J were used to test the Izod effect of soldered components. The microhardness of various welded samples was measured using a Vickers hardness tester according to ASTM 384.

2.5 Optical microscopy

Evaluation of the welded-area microstructure was done with an optical microscope (Moticam 1000, China) having a 25× lens zooming capacity. The specimens were cut in a sawing process with cooling water of a low temperature in the cutting zone to avoid grain refinement. The sectioned specimens were mounted with thermosetting resin for an effective edge retention. The mounted specimens were ground with an automated device, which consisted of a SiC abrasive sheet. The specimens were ground with a series of abrasive sheets of grit sizes ranging from 60 to 50. Fine diamond abrasives followed by colloidal alumina paste were used for mirror polishing. Potassium dichromate and a Keller solution were used as etching agents to reveal the grain structure of the Al alloy. Finally, the specimen surface was cleaned using distilled water and all the micrograph images were taken in polarized light.

3 RESULTS AND DISCUSSION

3.1 Mechanical properties

Tables 2 to **4** show the values of the tensile, notch tensile strength, Izod impact and hardness of weld beads. Tensile values were improved significantly for the square-wave tool-pin movement pattern. A weld was done at the tool rotation of 1500 min^{-1}, 1-mm step size, 150 mm/min weaving rate, and square tool-pin profile with a maximum strength factor of 99.82, which is larger than for the other process parameter weldments. This is because of the complete mixing of the two parent metals since the tool rotates for a longer time in the welding zone. When the tool moves in both x and y directions, the metals from the advancing side (Cu) and retreating side (aluminum) are completely mixed. Hence, intermetallic compounds like Mg, Si, Cr and Fe from aluminum were dispersed throughout the weld nugget. Similarly, the fusion of the parent metals generated the Al_4Cu_9 and Al_2Cu phases. The formation of many secondary phases in the matrix may arrest the crack propagation due to the polyphase strengthening method.[13,14] Similarly, when the axial load is applied the precipitated intermetallic compounds arrest the minute crack propagation through the grain boundaries. These phenomena help the metal to bear the maximum load.[15]

At the lower tool rotation (1500 min^{-1}) the grains are processed in a gentle manner and do not get affected by heat. Thus, the rate of creating the heat affecting the zones is minimum.[16] The maximum strength factor was achieved at the lower step size (1.0 mm) of the tool movement. This is because the maximum number of turns can be completed by the tool before it completes the full length of the weld on the plate. A fine mixture of parent metals reduces weld defects, improper mixing and poor cooling rate. Thus, the weld nuggets formed on the basis of the rotation of 1500 min^{-1}, 1.0 mm step size, 150 mm weaving rate and square tool-pin profile show distinct results when compared to the other nuggets. **Figure 3a** shows a tensile specimen based on the ASTM

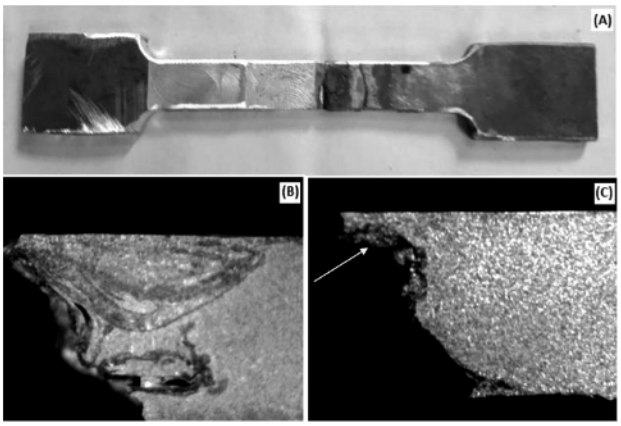

Figure 3: a) ASTM tensile specimen, b) brittle fracture on the advancing side, c) fracture on the retreating side

standard. **Figure 3b** shows a broken tensile specimen after the tensile test. A few dimples were observed, indicating some brittleness of the nugget due to the grains thermally affected during the joining process. **Figures 4a** to **4c** show the microhardness values of the welded part. It was noted that the maximum microhardness of 83 HV was achieved in the nugget zone obtained at 2000 min^{-1}, 1.0 mm step size, 150 mm/min weaving rate and with the square tool-pin profile. Grains were thermally affected at higher tool rotational speeds, causing increased brittleness and improved hardness. Thus, increased brittleness improves the hardness. Grains were refined at the nugget

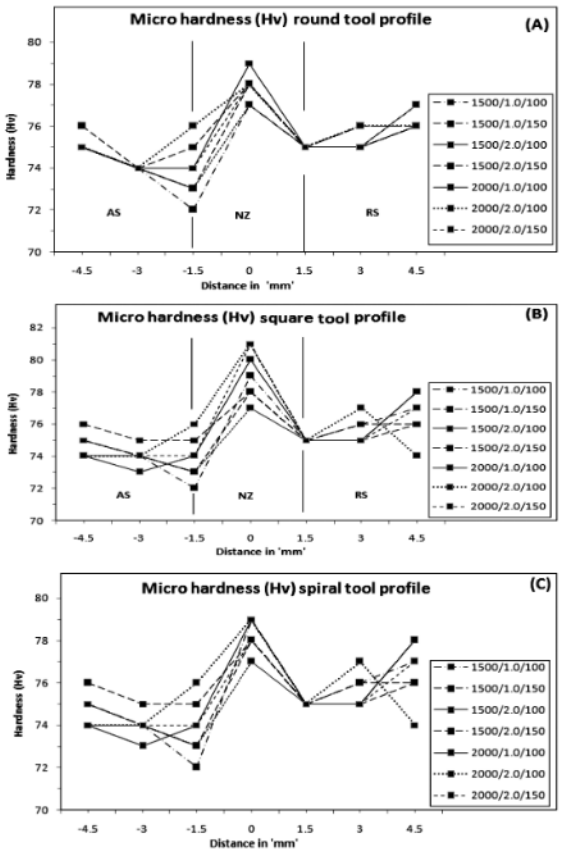

Figure 4: Microhardness values: a) round tool-pin profile, b) square tool-pin profile, c) spiral tool-pin profile

Table 2: Mechanical properties of Al 6061-Cu obtained with a round tool-pin profile

Rotation speed/S.S./ weaving rate	Tensile strength (MPa)	Normalized tensile strength (MPa)%	Notch tensile strength (MPa)	Normalized notch tensile strength (MPa)%	Yield strength (MPa)	Normalized yield strength (MPa)%	Impact strength (J)	Normalized impact strength (J)%	Strength factor %
1500/1.0/100	196	99.5	167	98.8	136	96.5	7.6	93.8	97.15
1500/1.0/150	194	98.5	169	100	132	93.6	7.9	97.5	97.42
1500/2.0/100	191	97.0	161	95.2	135	95.7	8.1	100	96.97
1500/2.0/150	195	99.9	164	97.0	138	97.8	8.1	100	98.67
2000/1.0/100	189	96.0	165	97.6	141	100	7.8	96.2	97.45
2000/1.0/150	197	100	165	98.8	136	96.4	7.5	92.5	96.92
2000/2.0/100	190	96.4	164	97.0	134	95.0	7.9	97.5	96.47
2000/2.0/150	189	96.0	167	98.8	132	93.6	8.0	98.7	96.77

Table 3: Mechanical properties of Al 6061-Cu obtained with a square tool-pin profile

Rotation speed/S.S/ weaving rate	Tensile strength (MPa)	Normalized tensile strength (MPa)%	Notch tensile strength (MPa)	Normalized notch tensile strength (MPa)%	Yield strength (MPa)	Normalized yield strength (MPa)%	Impact strength (J)	Normalized impact strength (J) %	Strength factor %
1500/1.0/100	199	92.9	168	96.5	139	100	7.9	94.0	95.85
1500/1.0/150	214	100	174	100	138	99.3	8.4	100	99.82
1500/2.0/100	196	91.6	166	95.4	135	97.1	8.0	95.2	94.82
1500/2.0/150	199	93.0	169	97.1	136	97.8	8.2	97.6	96.37
2000/1.0/100	195	91.1	167	95.6	139	100	7.7	91.6	94.57
2000/1.0/150	197	92.0	163	93.6	138	99.2	7.8	92.8	94.40
2000/2.0/100	196	91.6	168	96.5	136	97.8	7.9	94.0	95.00
2000/2.0/150	191	82.2	167	95.9	135	97.1	8.1	96.4	93.00

Table 4: Mechanical properties of Al 6061-Cu obtained with a spiral tool-pin profile

Rotation speed/S.S/ weaving rate	Tensile strength (MPa)	Normalized tensile strength (MPa) %	Notch tensile strength (MPa)	Normalized notch tensile strength (MPa) %	Yield strength (MPa)	Normalized yield strength (MPa) %	Impact strength (J)	Normalized impact strength (J) %	Strength factor %
1500/1.0/100	198	100	165	97.0	134	95.7	7.5	92.5	96.3
1500/1.0/150	197	99.5	170	100	136	97.1	7.7	95.0	97.9
1500/2.0/100	194	97.9	165	97.0	135	96.4	8.0	98.7	97.5
1500/2.0/150	192	96.9	167	98.2	136	97.1	7.8	96.3	97.1
2000/1.0/100	189	95.5	162	95.3	140	100	7.4	91.3	95.5
2000/1.0/150	190	95.9	161	94.7	137	97.8	7.6	93.8	95.5
2000/2.0/100	188	94.9	163	95.9	138	98.5	7.9	97.5	96.7
2000/2.0/150	189	95.4	163	95.9	136	97.1	8.1	100	97.1

and their cooling was slow, forming a finer grain size, which improved the hardness. A relatively low hardness was seen on the advancing side as a result of the coarse-grain formation.[17,18]

Due to the loop stirring of the nugget area allowed by the shorter wave length, an ultrafine grain structure was obtained. It is also observed on sample SS/1.0 with a maximum output of 144 MPa due to the compaction of fine-grain particles caused by continuous loop stirring in the matrix phase. This results in a layer boundary crack, shown in **Figure 3**, caused by the Orowan strengthening effect of the IMC particles present in the matrix stage of Al (**b**). In turn, this results in dislocation bowing in the phase line, enhancing the particle density to the ultrafine grain limit. This further increases the tensile modulus.[19]

Due to the dynamic recrystallization during the solidification process, the increase in the hardness creates harder IMC precipitates. According to the theory of molecular rigidity with topological restrictions, the atoms are bound by radial 2-body bonding constraints that fix

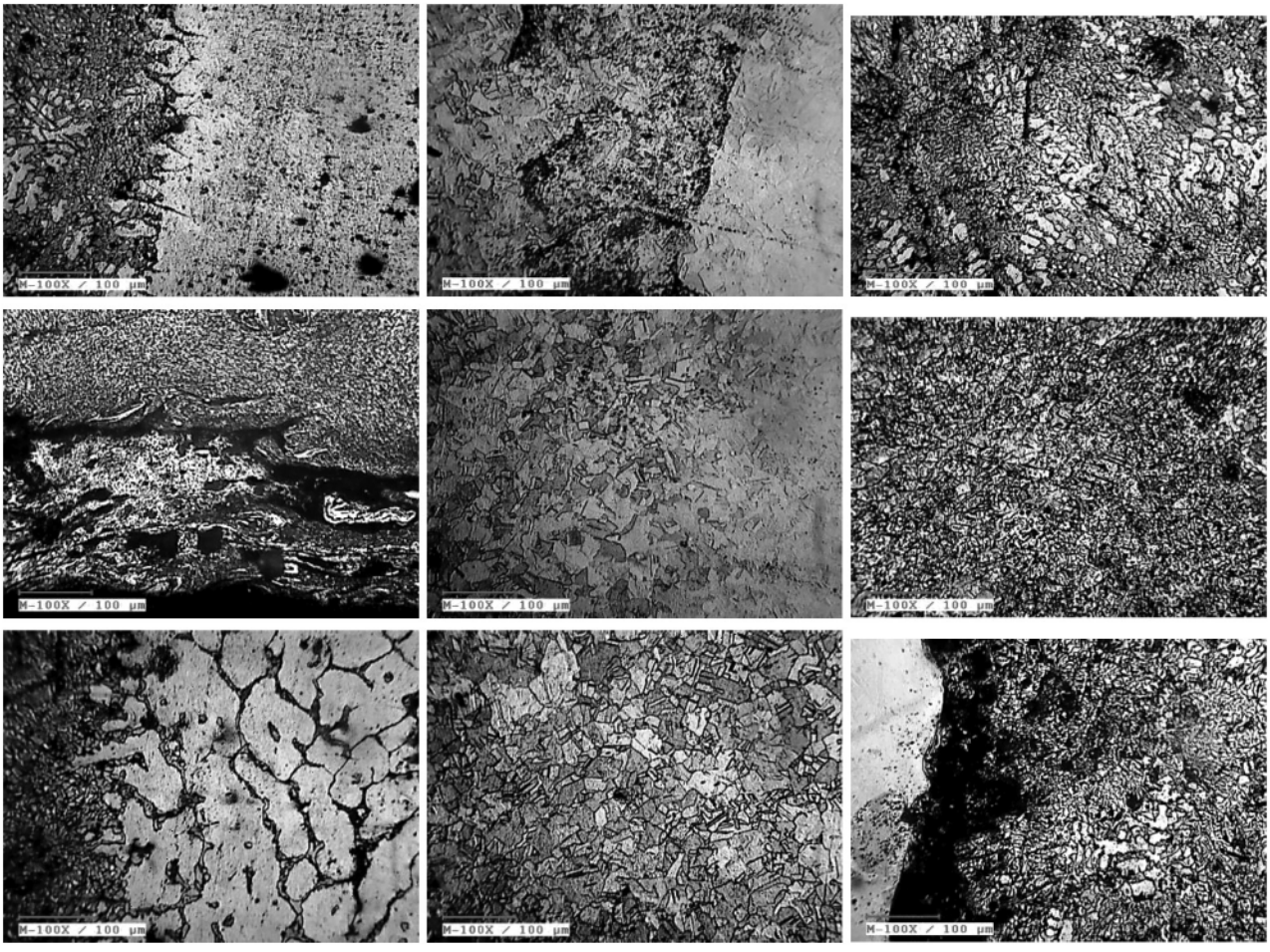

Figure 5: Cross-sectional microstructures of the weldments, formed with square-wave tool-pin movement

interatomic distances and angular 3-body bonding limitations that maintain an average angle fixed at the same time.[20] The formation of zeolitic frames, with the presence of spheroidal cementite IMCs, in the shear band of the nugget zone was found with microstructural observations and included in **Figure 3c**.

The decrease in the particle size based on the Hall-Petch mechanism was another parallel mechanism of the increase in the hardness value.[21]

3.2 Microstructure of joints

Figure 5 shows the cross-sectional microstructures of the weldments, formed with square-wave tool-pin movement and process parameters including the tool rotation of 1500 min^{-1}, 1.0 mm step size and 150 mm/min weaving rate along with the square tool-pin profile. **Figure 5a** also shows the microstructure of the AA 6061 parent metal. Particles of eutectics were seen along the tool direction. The fine particles are eutectics of Mg_2Si, spread over the weld nugget, improving the load-bearing capability. Even distribution was a result of the square wave path of the tool movement on the processed zone. The x-y traverse movement of the tool enabled the complete mixing of the parent metals with each other. **Figure 5b** shows the field near the processed zone with large particles of Mg_2Si in the primary aluminum alloy matrix.[22] **Figure 5c** shows the interface junction of a parent metal with severely heated and recrystallized larger grains of primary aluminum with eutectics at the grain boundaries. **Figure 5d** shows another field with the HAZ of the base metal and the rapidly plasticized and cooled matrix of AA 6061. It reveals the brittleness of the nugget zone compared to the other areas. Hence, a greater hardness was experienced. **Figure 5e** shows the rapidly plasticized and cooled zones with Al-Si and Mg_2Si. The constituents were seen spread over the weld nugget zone and an increase in the load-bearing capacity of the weld nugget via precipitated strengthening was found.[23,24]

Figure 5f shows interface junctions of the fused zone and the melted zone of the aluminum and copper HAZ. The fused zone is dark, with the constituents of both copper and AA6061, indicating a fine mixture of the base metals. The copper zone shows completely dissolved alpha grains and a fine beta phase. **Figure 5g** shows the interface of a parent metal, copper, and the HAZ of copper. Partial recrystallization of the copper solid solution was observed. **Figures 5h** and **5i** show grains of copper near the HAZ with larger grains of the copper solid solution due to the grain growth. This is because highly thermally affected grains took a longer time to cool down. Hence, the grains grew significantly. **Figures 5h** and **5i** include the microstructure of the copper base metal from the HAZ and the area close to the unaffected zone. Thus, it can be stated that the formation of the fine mixture of Al and Cu in the weld-nugget zone was, based on the microstructure images, a result of complete mixing via the square-wave pattern. The square tool-pin profile allowed the base metals to mix completely due to orthogonal stirring. When the tool geometry is perpendicular to the workpiece material, the contact area and the coefficient of friction of metal are high. This phenomenon helps the processed zone grains to get reoriented and mix thoroughly on the weldments.[25,26]

Figure 6 shows x-ray results for dissimilar metals of aluminum and copper. **Figures 6a** and **6b** show that there was no weld flaw within the weldment, indicating a fine and uniform grain formation and proper cooling.[27]

The formation of spheroidal cement with much higher precipitation was observed. Some intermetallic Al compounds, like Al_2Cr_4, were found in this region to a greater extent. Additional agitation helps to break oxide layers regularly, causing the formation of fine grains. The existence of the precipitates of Mg_2Si strengthened the nugget region. All the images show that all grains move in the direction of the tool. It is clear from every image that in a square-wave tool process, the grains and intermetallic compounds are arranged, rotated and uniformly distributed on the Al matrix, thus having no defects in the welded part.

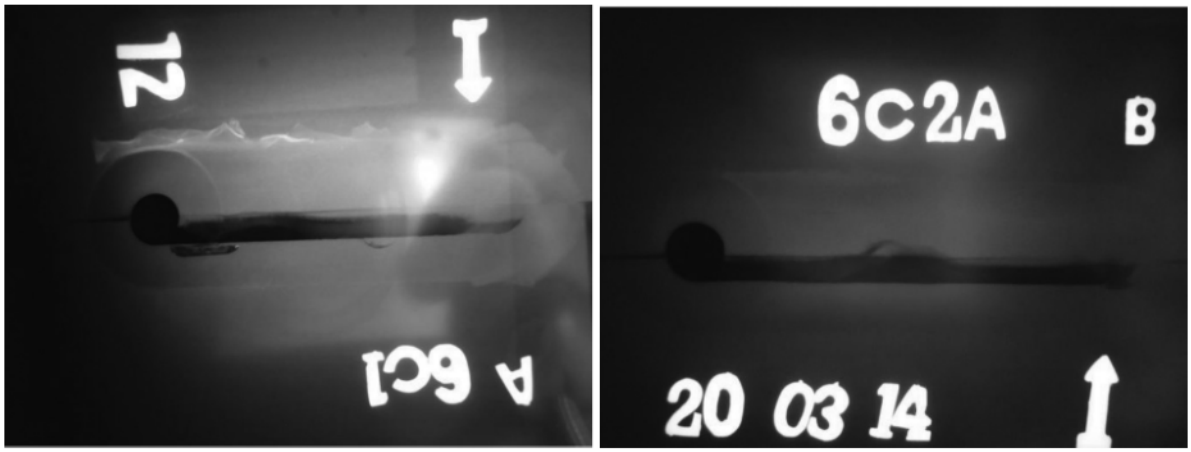

Figure 6: Radiographs of the welded Al-Cu alloy: a) defect-free weld, b) tunnel-defect weld

3.3 Energy dispersive spectrum analysis

Figure 7a to **7c** show the EDAX analysis of the advancing side, nugget zone and retreating side of the processed zones. However, the advancing side has grains of primary aluminum, whereas the nugget zone has a eutectic mixture of both aluminum and copper. Similarly, the retreating side has grains of copper, indicating a complete fusion of the two parent metals at the nugget with the formation of new crystals of both Al and Cu. **Figure 7a** shows the EDAX report for the retreating side. It shows the presence of raw aluminum on the retreating side, indicating the absence of copper. **Figure 7b** shows the EDAX report for the nugget with both aluminum (45 %) and copper (35 %) while the remaining elements were oxides of Al and Cu. The microconstituents were dispersed throughout the nugget zone. The oxide formation was due to heavy heat dissipation during machining. Similarly, **Figure 7c** shows raw copper on the advancing side.

4 CONCLUSIONS

The results obtained lead to the following conclusions. The square-wave tool path pattern can be successfully implemented and welding can be done at different parameters. The process parameters including the tool rotation of 1500 min^{-1}, 1-mm step size and 150 mm/min weaving rate along with the square tool-pin profile provide for the highest strength compared to the other process parameters. The microstructure images reveal a uniform grain flow and an even dispersion of microconstituents in all directions. The square-wave tool-pin pattern made the weldments defect-free due to complete mixing of the parent metals and allowed uniform cooling. X-ray results show a flaw-free weldment of aluminum and copper. The EDAX analysis reveals the presence of the grains of both copper and aluminum at the nugget. Hence, the square-wave tool-pin movement pattern during friction stir welding provides useful results for both the mechanical properties and microstructure of the welded AA6061-Cu alloy system. The selected process parameters including the tool rotation of 1500 min^{-1}, 1-mm step size (x-y tool movement) and 150 mm/min weaving rate could be considered for better weldment qualities.

5 REFERENCES

[1] H. Shens, H. J Liu, Effect of welding speed on microstructure and mechanical properties of friction stir welded copper, Materials and Design, 31 (**2010**), 3937–3942, doi:10.1016/j.matdes.2010.03.027

[2] S. Vijayan, R. Raju, S. R. K. Rao, Multi objective optimization of friction stir welding process parameters on aluminum alloy AA 5083

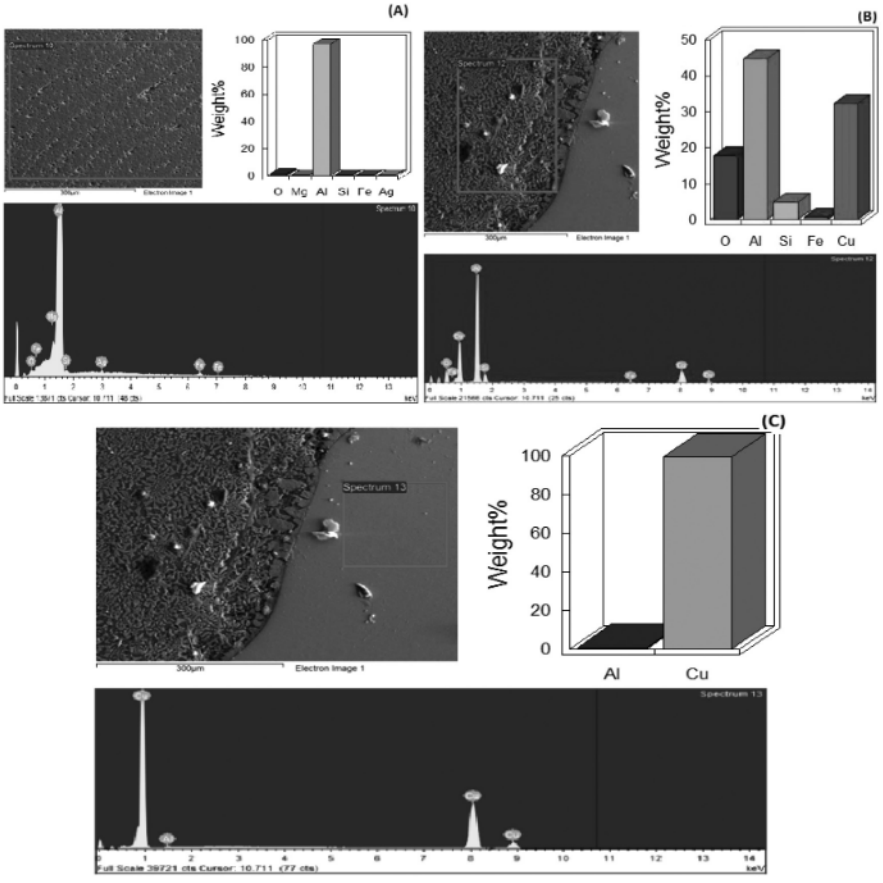

Figure 7: EDAX reports: a) retreating side, b) nugget zone, c) advancing side of the processed zone

using Taguchi-based grey relation analysis, Mater. Manuf. Process., 25 (**2010**), 1206–1212, doi:10.1080/10426910903536782

[3] N. Z. Khan, Zahid. A. Khan, A. N. Siddiquee, Effect of shoulder diameter to pin diameter (D/d) ratio on tensile strength of friction stir welded 6063 aluminium alloy, Materials Today: Proceedings, 2 (**2015**) 4–5, 1450–1457, doi:10.1016/j.matpr.2015.07.068

[4] R. I. Rodriguez, J. B. Jordon, P. G. Allison, T. Rushing, L. Garcia, Microstructure and mechanical properties of dissimilar friction stir welding of 6061-to-7050 aluminum alloys, Mater. Des., 83 (**2015**), 60–65, doi:10.1016/j.matdes.2015.05.074

[5] R. P. Mahto, R. Bhoje, S. Pal, K. Joshi, S. Harshadeep, S. Das, A study on mechanical properties in friction stir lap welding of AA 6061-T6 and AISI 304, Materials Science and Engineering A, 652 (**2016**), 136–144, doi:10.1016/J.MSEA.2015.11.064

[6] J. Mohammadi, Y. Behnamian, A. Mostafaei, H. Izadi, T. Saeid, A. H. Kokabi, A. P. Gerlich, Friction stir welding joint of dissimilar materials between AZ31B magnesium and 6061 aluminum alloys: Microstructure studies and mechanical characterizations, Materials Characterization, 101 (**2015**), 189–207, doi:10.1016/j.matchar.2015.01.008

[7] S. Babu, K. Elangovan, V. Balasubramanian, M. Balasubramanian, Optimizing Friction Stir Welding Parameters to Maximize Tensile Strength of AA2219 Aluminum Alloy Joints, Metals and Materials International, 15 (**2009**) 2, 321–330, doi:10.1007/s12540-009-0321-3

[8] Q. Zhengzhang, W. Biao, W. Liu, Microstructure and mechanical properties of dissimilar Al-Cu joints by friction stir welding, Trans. Nonferrous Met. Soc., 25 (**2015**), 1779–1786, doi:10.1016/S1003-6326(15)63783-9

[9] H. Bisadi, A. Tavakoli, M. T. Sangsaraki, K. T. Sangsaraki. The influences of rotational and welding speeds on microstructures and mechanical properties of friction stir welded Al5083 and commercially pure copper sheets lap joints, Materials and Design, 43 (**2013**), 80–88, doi:10.1016/j.matdes.2012.06.029

[10] D. Jayabalakrishnan, M. Balasubramanian, Eccentric-weave friction stir welding between Cu and AA 6061-T6 with reinforced graphene nanoparticles, Materials and Manufacturing Processes, 33 (**2018**) 3, 333–342, doi:10.1080/10426914.2017.1339323

[11] M. Balasubramanian, D. Jayabalakrishnan, Influence of Pin Offset and Weave Pattern on the Performance of Al-Cu Joints Reinforced with Graphene Particles, Int. J. of Aut. and Mech. Eng., 17 (**2020**) 3, 8186–8196, doi:10.15282/ijame.17.3.2020.12.0616

[12] M. Cabibbo, A. Forcellese, M. Simoncini, M. Pieralisi, D. Ciccarelli, Effect of welding motion and pre-/post-annealing of friction stir welded AA5754 joints, 93 (**2015**), 146–159, doi:10.1016/j.matdes.2015.12.099

[13] M. Ghosh, K. Kumar, R. S. Mishra, Friction stir lap welded advanced high strength steels: microstructure and mechanical properties, Mater. Sci. Eng. A, 528 (**2011**), 8111–8119, doi:10.1016/j.msea.2011.06.087

[14] Z. Saeid, A. Abdollah-Zadeh, B. Sazgari, Weldability and mechanical properties of dissimilar aluminum–copper lap joints made by friction stir welding, Journal of Alloys Compound, 490 (**2010**) 1–2, 652–655, doi:10.1016/j.jallcom.2009.10.127

[15] H. K. Mohanty, M. M. Mahapatra, P. Kumar, P. Biswas, N. R. Mandal, Modeling the effect of tool shoulder and probe profile geometries on friction stirred aluminum welds using RSM, J. Marine Sci. Appl., 11 (**2012**), 493–503, doi:10.1007/s11804-012-1160-z

[16] Y. C. Chen, K. Nakata, Microstructural characterization and mechanical properties in friction stir welding of aluminum and titanium dissimilar alloys, Mater. Des., (**2009**) 30, 469–474, doi:10.1016/j.matdes.2008.06.008

[17] Z. L. Hu, X. S. Wang, Q. Pang, F. Huang, X. P. Qin, L. Hua, The effect of post processing on tensile property and microstructure evolution of friction stir welding aluminium alloy joint, Materials Characterization, 99 (**2015**), 180–187, doi:10.1016/j.matchar.2014.11.015

[18] P. Xue, G. M. Xie, B. L. Xiao, Z. Y. Ma, L. Geng, Effect of heat input conditions on microstructure and mechanical properties of friction-stir-welded pure copper, Metall. Mater. Trans. A, (**2010**) 41, 2010–2021, doi:10.1007/s11661-010-0254-y

[19] M. Stepniewska, K. Januchta, C. Zhou, A. Qiao, M. M. Smedskjaer, Y. Yue, Observation of indentation-induced shear bands in a metal-organic framework glass, Proceedings of the National Academy of Sciences, 117 (**2020**) 19, 10149–10154, doi:10.1073/pnas.2000916117

[20] L. Trueba, G. Heredia, L. B. Johannes, Effect of tool shoulder features on defects and tensile properties of friction stir welded aluminium 6061-T6, Journal of Material Processing Technology, 12 (**2015**), 455–561, doi:10.1016/j.jmatprotec.2014.12.027

[21] S. N. Naik, S. M. Walley, The Hall–Petch and inverse Hall–Petch relations and the hardness of nanocrystalline metals, J. Mater. Sci., 55 (**2020**), 2661–2681, doi:10.1007/s10853-019-04160-w

[22] I. Shigematsu, Y. J. Kwon, K. Suzuki, T. Imai, N. Saito, Joining of 5083 and 6061aluminum alloys by friction stir welding, Journal of Material Science Letters, (**2003**) 22, 353–356, doi:10.1023/A:1022688908885

[23] L. Karthikeyan, V. S. Senthilkumar, K. A. Padmanabhan, On the role of process variables in the friction stir processing of cast aluminium A319 alloy, Mater. Des., 31 (**2010**), 761–71, doi:10.1016/j.matdes.2009.08.001

[24] P. Joswik, L. Śnieżek, Experimental Analysis of Crack Growth in a Notched Specimen Made of Ni_3Al Intermetallic Alloy, Journal of Notch Effect and Fracture, 11 (**2001**), 257–269, doi:10.1007/978-94-010-0880-8_16

[25] Z. Azari, C. Casavola, Characterization and prediction of cracks in coated materials, International scholarly research notice, (**2015**), 197–207, doi:10.1155/2015/594147

[26] P. Xue, B. L. Xiao, D. R. Ni, Z. Y. Ma, Enhanced mechanical properties of friction stir welded dissimilar Al-Cu joint by intermetallic compounds, Journal of Materials Science and Engineering A, (**2010**) 527, 5723–5727, doi:10.1016/j.msea.2010.05.061

[27] H. J. Liu, J. J. Shen, L. Zhou, Y. Q. Zhao, C. Liu, L. Y. Kuang, Microstructural characterization and mechanical properties of friction stir welded joints of aluminum alloy to copper, Journal of Science and Technology of Welding and Joining, (**2011**) 16, 92–99, doi:10.1179/1362171810Y.0000000007